The Oxidation State of [4Fe4S] Clusters Modulates the DNA-Binding Affinity of DNA Repair Proteins

Edmund C. M. Tse, Theodore J. Zwang, Jacqueline K. Barton[*]

Division of Chemistry and Chemical Engineering, California Institute of Technology, Pasadena, California 91125, United States

**Table of Contents:**

Supplementary Figures & Tables

Figure S1 displays cyclic voltammograms (CVs) of a DNA-modified Au electrode in DNA buffer with EndoIII in various concentrations in solution. The current of the redox wave increases as a function of increasing EndoIII concentration, further supporting the notion[1] that the redox wave is likely related to EndoIII in solution. 1 μM was chosen for bulk electrolysis to increase oxidation yield.
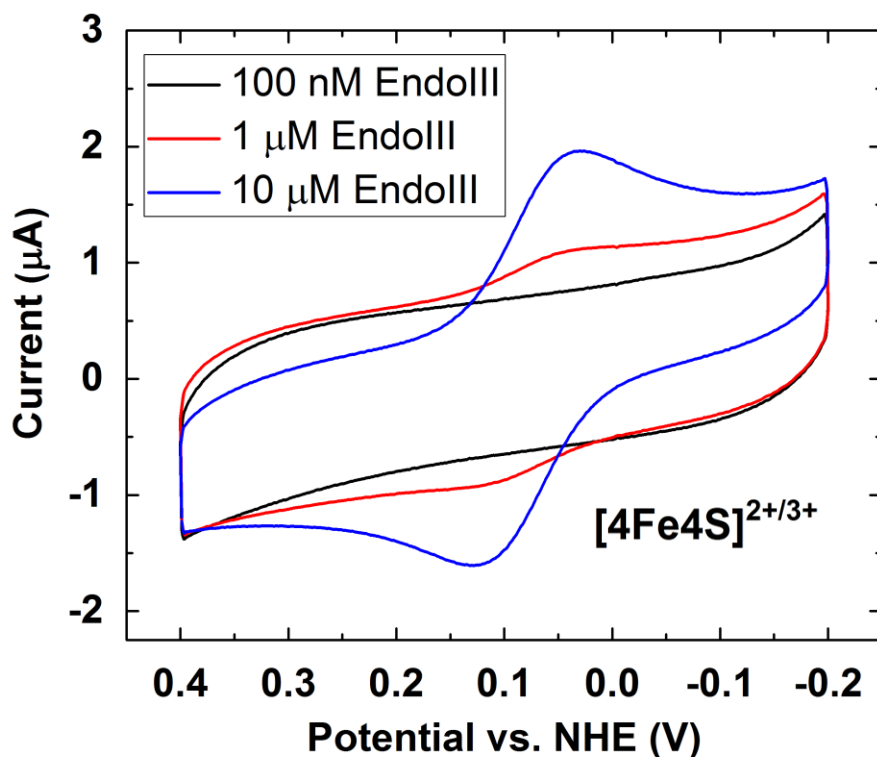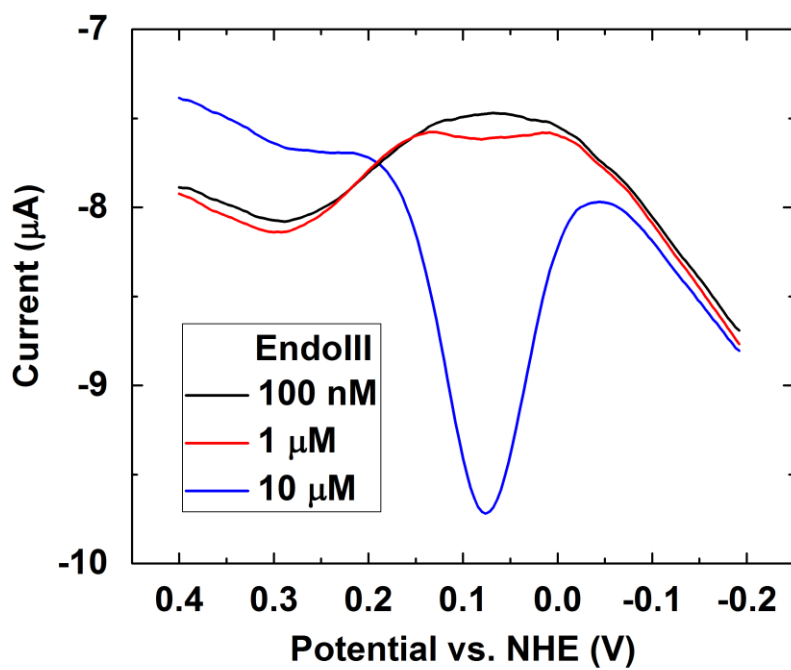

Figure S1. Cyclic voltammetry of EndoIII on a DNA-modified electrode. CVs in DNA buffer (pH 7.0, 5 mM NaH$_2$PO$_4$, 50 mM NaCl) with 100 nM EndoIII (black), 1 μM EndoIII (red), and 10 μM EndoIII (blue) added at a scan rate of 100 mV/s. E_{mid} = +80 mV vs. NHE.
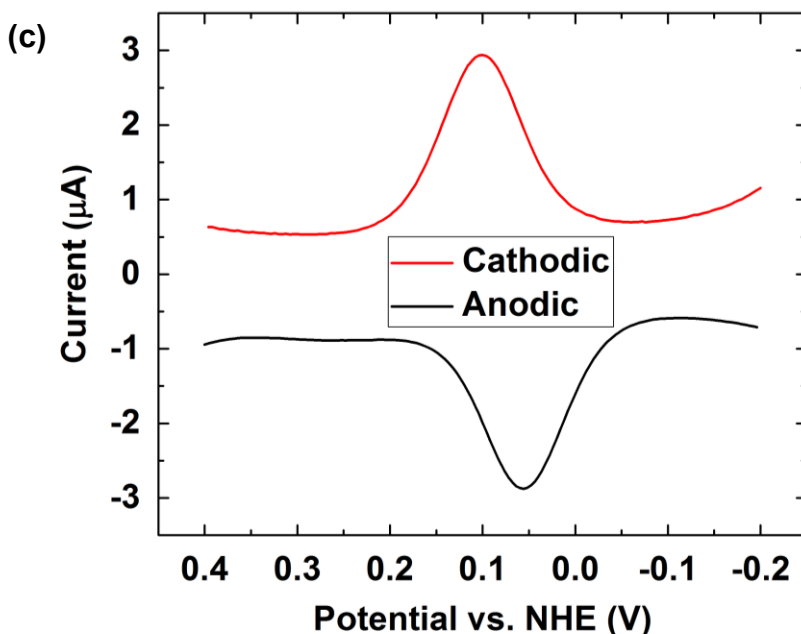
Square wave voltammetry (SWV) and differential pulse voltammetry (DPV) eliminate background capacitive current, thereby allowing the redox peak to be visualized with relative ease (Figure S2).

(a)
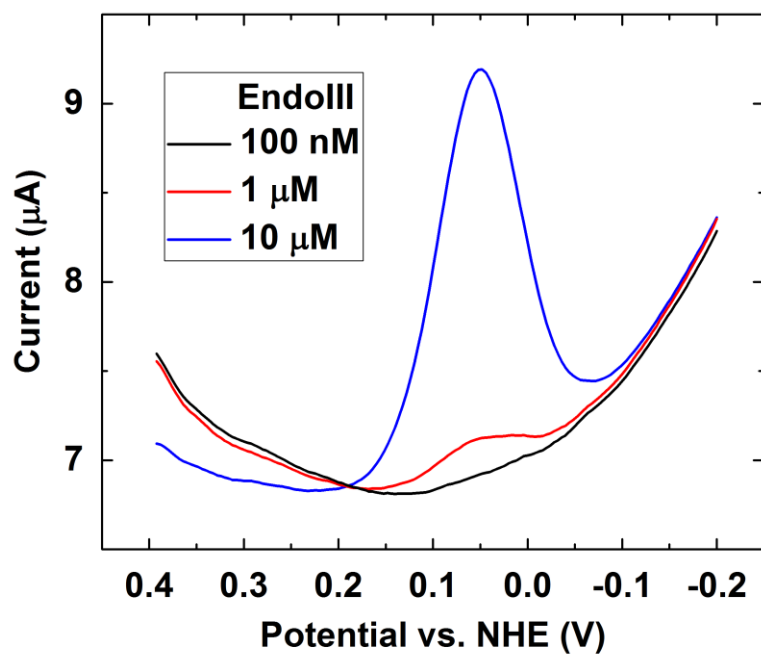
(b)

Figure S2. Square wave voltammetry (SWV) and differential pulse voltammetry (DPV) of EndoIII on a DNA-modified electrode. (a) Cathodic and (b) anodic SWVs in DNA buffer (pH 7.0, 5 mM NaH$_2$PO$_4$, 50 mM NaCl) with 100 nM EndoIII (black), 1 μM EndoIII (red), and 10 μM EndoIII (blue) added. (C) Cathodic (red) and anodic (black) DPVs in DNA buffer (pH 7.0, 5 mM NaH$_2$PO$_4$, 50 mM NaCl) with 10 μM EndoIII added.

To determine if the redox reaction of EndoIII on DNA-modified electrodes is a diffusionless or a diffusive process, we conducted Randles-Sevcik analysis by measuring the peak current responses at various scan rates while holding the concentration of EndoIII in solution constant (Figure S3). In Figure S4b, a poor linear relationship is observed for the Randles-Sevcik plot of EndoIII with the peak current versus the scan rate, indicating that the redox event does not originate from a surface-bound species and that EndoIII does not adsorb very strongly onto DNA-modified electrodes under this condition. By contrast, the peak currents of both the anodic and cathodic peaks scale with the square root of the scan rate (Figure S4a), indicating that under these conditions the redox reaction of EndoIII is in a diffusion-controlled regime. Therefore, at concentrations at or below 10 μM, EndoIII likely diffuses from the bulk solution to the electrode surface to undergo redox reaction upon binding to DNA and then diffuses back into the bulk solution to allow for freshly exposed DNA surfaces for other copies of EndoIII to approach and participate in subsequent redox events.
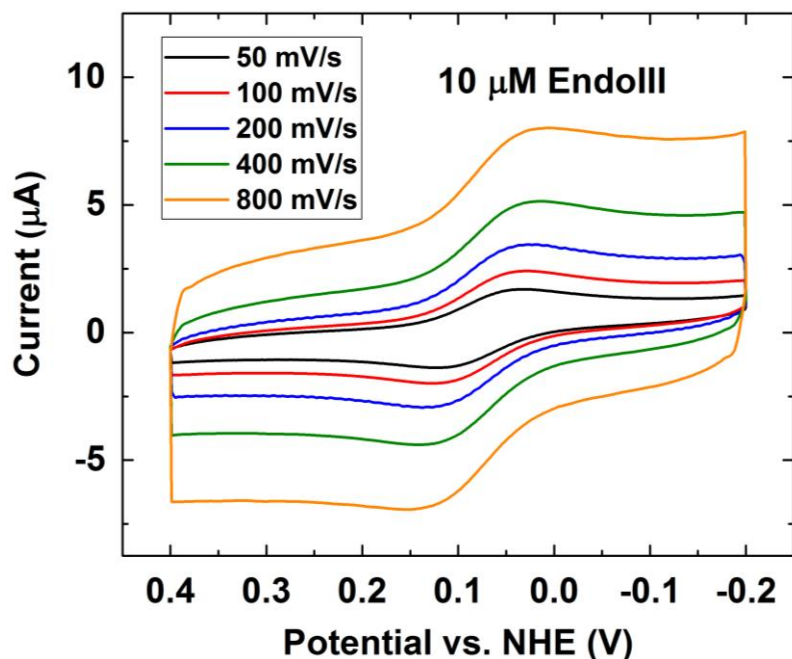
Figure S3a. Cyclic voltammetry of EndoIII on a DNA-modified electrode with varying scan rates. CVs in DNA buffer (pH 7.0, 5 mM NaH_2PO_4, 50 mM NaCl) with 10 μM EndoIII added at a scan rate of 50 (black), 100 (red), 200 (blue), 400 (green), and 800 (orange) mV/s. 10 μM is chosen as the concentration to allow for clear visualization of the redox waves.
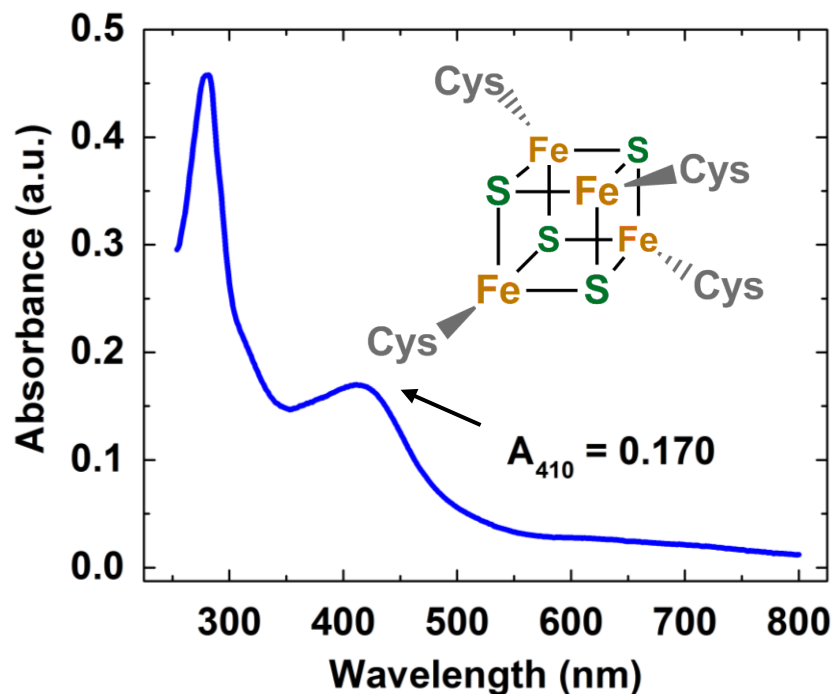
Figure S3b. UV-visible absorbance spectra of EndoIII. The [4Fe4S] redox cofactor exhibits an ε of 17,000 M^{-1} cm^{-1} at 410 nm.[2] Cluster loading was at least 70%.
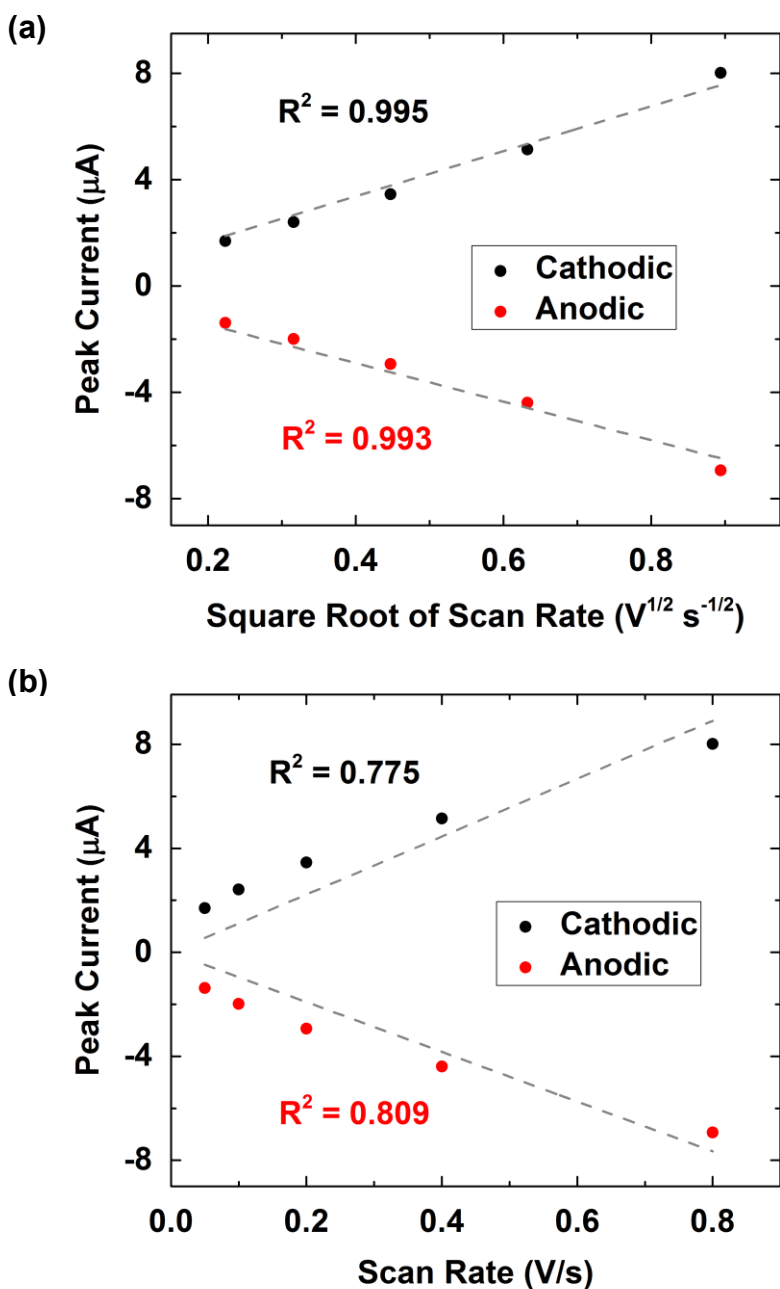
Figure S4. Randles-Sevcik plots of the peak currents of EndoIII. Randles-Sevcik plots of the peak currents of 10 μM EndoIII at various scan rates recorded in Figure S3a versus (a) the square root of the scan rate, and (b) the scan rate.

To check if the protein structure is altered by the bulk electrolysis process, we monitored qualitatively the changes to the secondary structure of EndoIII by circular dichroism (CD).
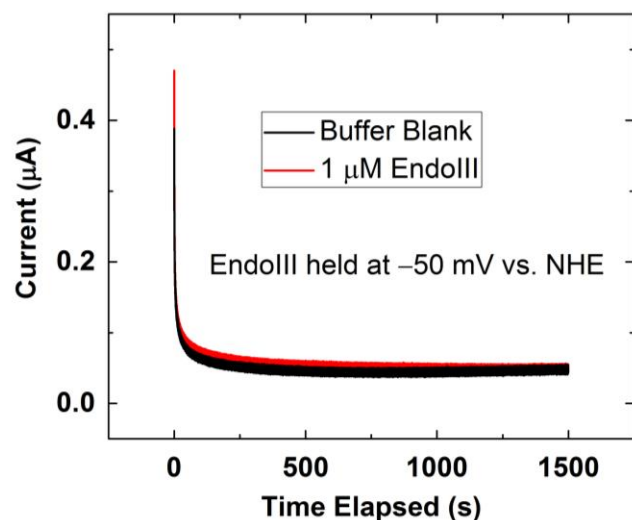
Figure S5a. Bulk electrolysis in DNA buffer (pH 7.0, 5 mM NaH_2PO_4, 50 mM NaCl, black line) with 1 μM EndoIII added (red line) held at −50 mV vs. NHE. Only a small portion of the proteins present in the solution was reduced, suggesting that the native or as-isolated oxidation state of the protein is primarily in the reduced $[4Fe4S]^{2+}$ state.
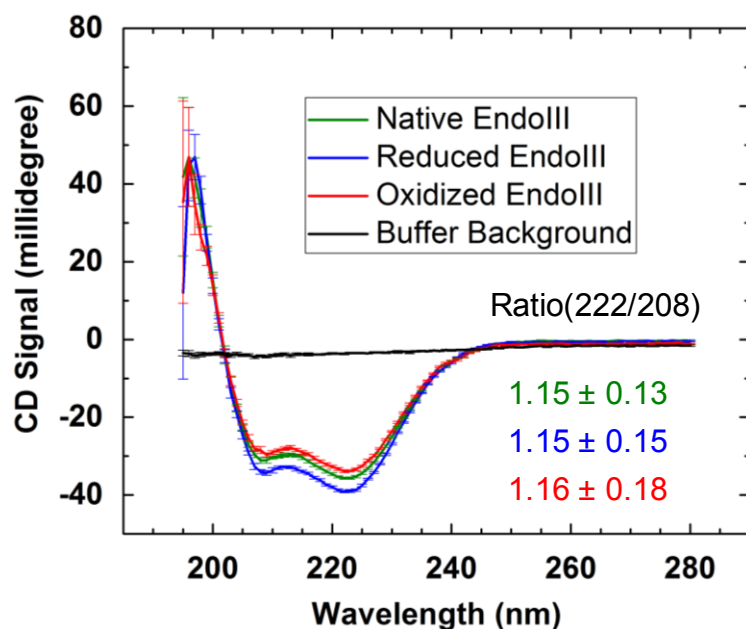
Figure S5b. The influence of bulk electrolysis on EndoIII structure as monitored by circular dichroism. CD spectra of DNA buffer (pH 7.0, 5 mM NaH_2PO_4, 50 mM NaCl, black line) with native (green), reduced (blue), and oxidized (red) EndoIII (5 μM, 1000 μL) added. The slight change in signal intensity is likely due to a change in the optical density. Measuring the ratio of the CD signal at 222 nm to that at 208 nm is typically used to analyze α-helical proteins. Coiled

coils and isolated α-helix exhibit ratios of 1.1 and 0.9, respectively. Here, native, reduced, and oxidized EndoIII exhibit ratios of ca. 1.15, suggesting that EndoIII retains its coiled coils and that the overall structure of EndoIII is not perturbed by bulk electrolysis.
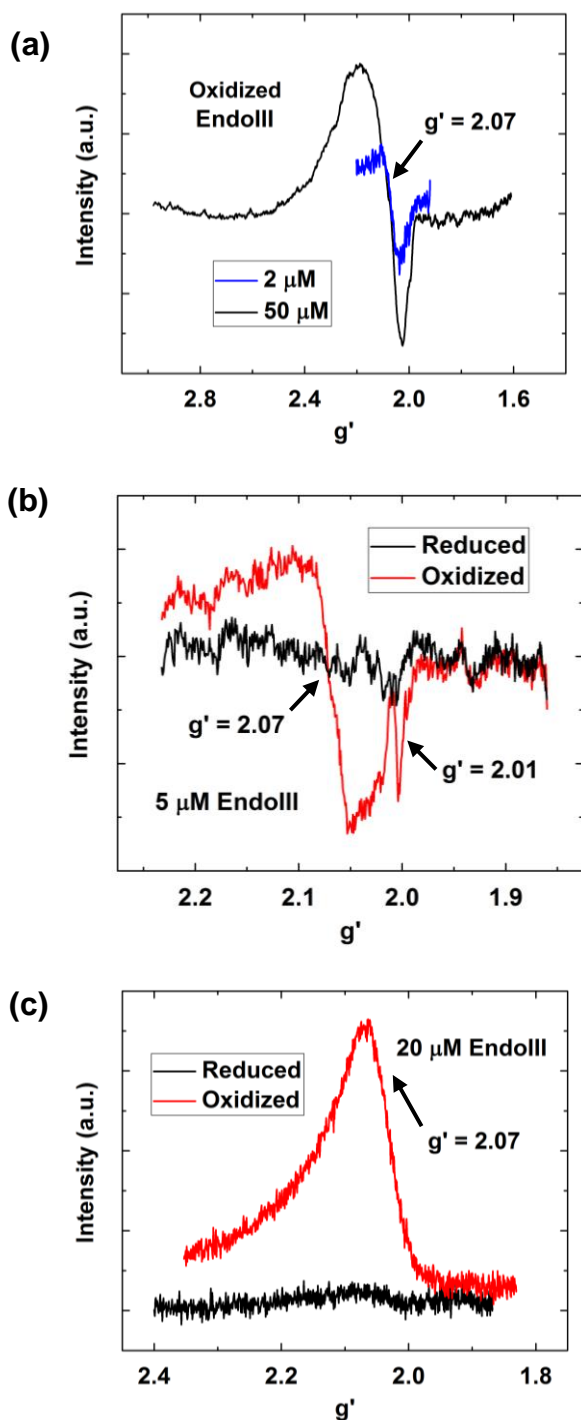
Figure S6. Continuous wave (CW) electron paramagnetic resonance (EPR) spectra of EndoIII. (a)

2 μM (blue) and 50 μM (black) oxidized EndoIII prepared under anaerobic conditions, (b) reduced (black) and oxidized (red) 5 μM EndoIII exposed to ambient air, and (c) pulse electron spin echo envelope modulation (ESEEM) spectra of reduced (black) and oxidized (red) 20 μM EndoIII in protein buffer (20 mM NaH_2PO_4 pH 7.5, 100 mM NaCl, 5% glycerol, 1 mM EDTA). Instrument settings: modulation amplitude = 10 G at 100 kHz; frequency = 9.37 GHz; microwave power = 4.7 mW; and temperature = 10 K.

In Figure S6, for samples prepared under an N_2 atmosphere, an absence of an EPR signal with a g value of 2.01 indicates that no detectable $[3Fe4S]^{1+}$ degradation product was generated. As a positive control, for the oxidized EndoIII sample that was exposed to O_2 by passive diffusion in ambient air, we observed an EPR signal at a g value of 2.01, which is indicative of the presence of degraded $[3Fe4S]^{1+}$ clusters.[2]

EndoIII	# of DNA strands	# of Proteins	Proteins:DNA
< 1 % Ox	84	120	1.43
33 % Ox	243	368	1.51
66 % Ox	129	229	1.78
> 99 % Ox	395	844	2.14

Table S1. Probing DNA-protein interactions using AFM. Summary of the average number of proteins bound on DNA versus the number of DNA strands counted.

Table S1 displays the number of pUC19 DNA strands observed, the number of EndoIII bound on the countable DNA strands, and the calculated ratio of EndoIII:pUC19. The results show that as EndoIII becomes more and more oxidized, the protein:DNA ratio increases (Figure 2b). Binding affinity (K_D) can be calculated from this set of AFM data using Eq. S1-3.

$$\% \; Protein \; bound \; on \; DNA = \frac{\# \; of \; Proteins \; bound \; on \; DNA}{Total \; \# \; of \; Proteins} = \frac{[P]}{[P] + K_D} \quad Eq.\, S1$$

Rearranging Eq. S1 gives Eq. S2.

$$K_D = \frac{[P] - \% \; Protein \; bound \; on \; DNA \times [P]}{\% \; Protein \; bound \; on \; DNA} \quad Eq.\, S2$$

$$Relative\ binding\ affinity\ between\ proteins\ A\ and\ B = \frac{K_{D,A}}{K_{D,B}} \qquad Eq.\,S3$$

(a)

(b)
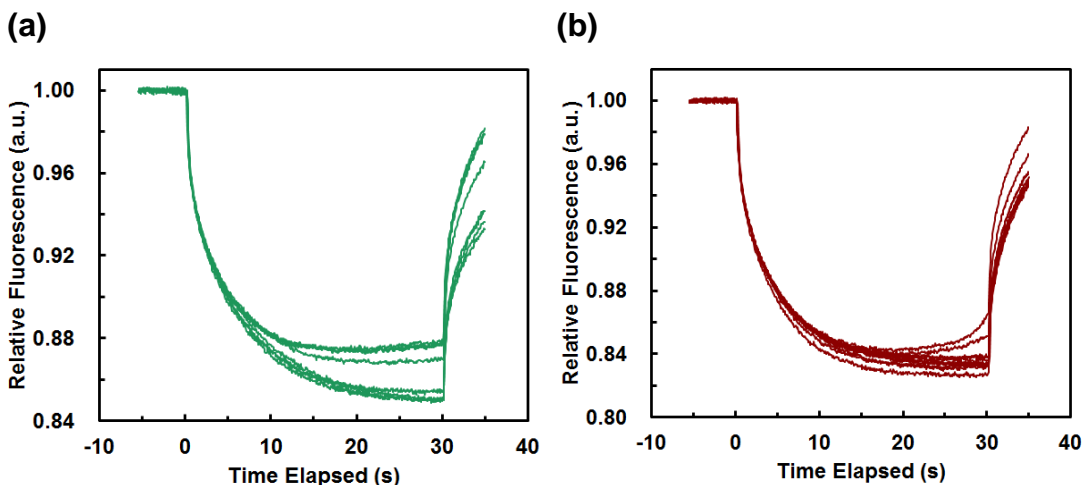
Figure S7. Microscale thermophoresis of EndoIII. MST plots of (a) native and (b) oxidized EndoIII.

Electrophoretic mobility shift assay (EMSA) is commonly used to measure the binding affinity between proteins and DNA. However, the EMSA experimental setup, even when conducted in an anaerobic chamber at 4 °C, is not compatible with oxidized EndoIII. The [4Fe4S] clusters of DNA repair proteins in the oxidized state degrade in the presence of O_2. Efforts including pre-running gel in degassed buffer and then switching to freshly-degassed buffer prior to protein loading were not successful. The amount of O_2 generated by the Pt electrodes during the gel running process resulted in cluster degradation. For an EMSA gel-shift experiment, about 20 pmol (10 μL per lane) of protein is typically used. The amount of O_2 generated per second during a gel-shift experiment is about 10 μmol (= 50 V × 0.02 A × 1 s × 1 mol / 96485 C), and the total amount of O_2 generated over the course of a 4-hour EMSA gel-shift experiment is about 37 mmol. Since the solubility of O_2 in aqueous solution is about 1.2×10^{-6} mol cm^{-3}, the maximum amount of dissolved O_2 saturated in 1 L TBE buffer is ca. 1.2 mmol. The O_2 diffusion coefficient in aqueous medium is about 1.9×10^{-5} cm^2 s^{-1}. The amount of O_2 liberated during a gel-shift experiment is more than enough to saturate the running buffer with O_2. Accordingly, oxidized EndoIII likely is overwhelmed by O_2 generated *in situ* during the gel running process. ITC measurements show a 28× increase in the affinity of the predominantly oxidized protein sample for DNA when compared to the predominantly reduced sample. However, instrument limitation prevented ITC from being

operated anaerobically. We therefore switched to using MST to determine the DNA binding affinity of EndoIII. MST is a technique that allows for anaerobic determination of the binding affinity of O_2-sensitive proteins such as FeS cluster biogenesis machinery to their substrates.[3] We utilized MST to probe the binding affinity of EndoIII to DNA in different redox states. MST results show that oxidized EndoIII with $[4Fe4S]^{3+}$ cluster binds 21-mer dsDNA ca. 550 times stronger than EndoIII predominantly in the reduced state (Figure S7). This comparison may understate the true difference in affinity between the reduced and oxidized proteins, because it is unlikely that bulk electrolysis has completely removed all oxidized protein from the reduced sample. The presence of a small amount of oxidized protein will convolute the affinity measurement in any sample, even when the oxidized protein is in low concentration compared to the reduced protein, because the oxidized protein has a significantly higher affinity for DNA. This phenomenon infers that the values measured by MST that show a $550\times$ change in affinity between the two protein redox states may be obfuscated by a change in the amount of oxidized protein present in the sample. Calculating the 99% confidence interval for the ratio of measured affinities suggests that the oxidized sample has between $276\times$ and $1157\times$ increase in affinity over the reduced sample.
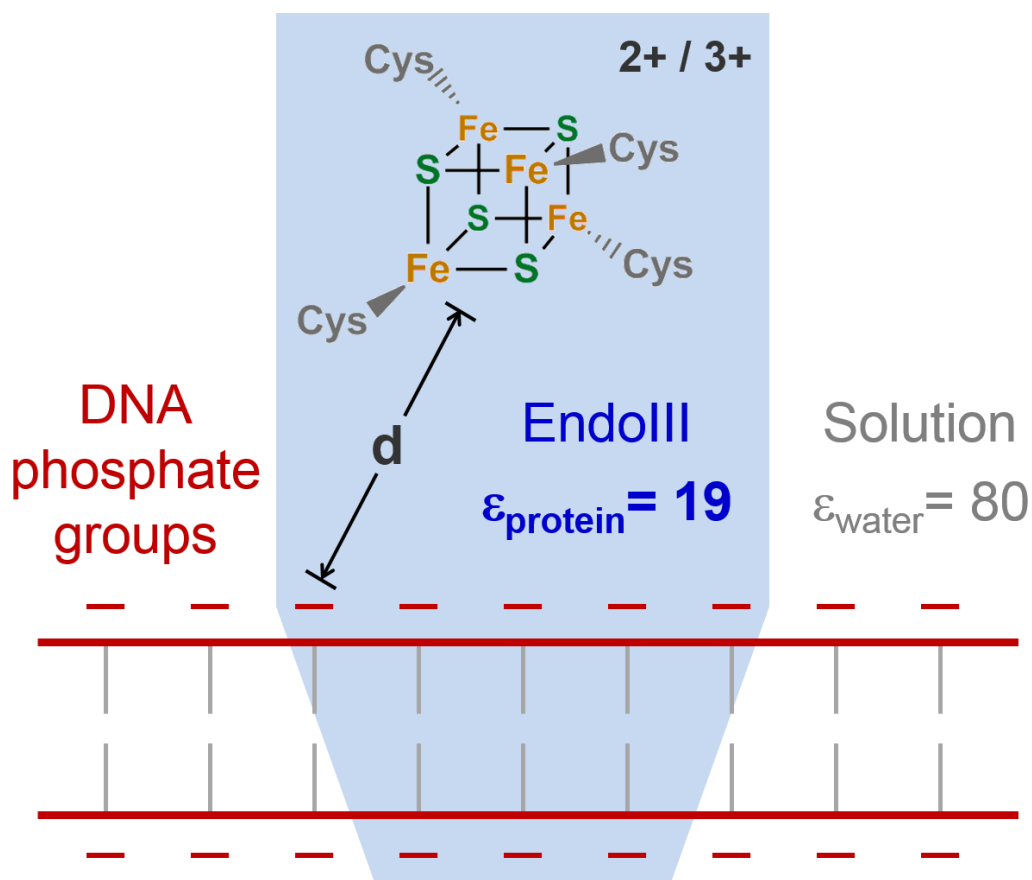
Figure S8. A model describing the electrostatic interactions between EndoIII and DNA.

The crystal structure (PDB:1ORN) revealed that eight phosphates on the DNA backbone interact with the amino acid residues of EndoIII. The average distance between the redox-active metallocofactor and the eight phosphate groups is about 18 Å. The neighboring phosphate groups that do not directly interact with the protein binding surface are not crucial in this calculation because (1) PE $\propto$ 1/d, (2) d increases for phosphate groups further away from the [4Fe4S] cluster, and (3) the dielectric constant (ε_r) between the two point charges needs to take into account of the intervening water molecules that have a ε_r of 80. The electrostatic nature of the binding surface between EndoIII and DNA were predicted in another crystal structure (PDB: 2ABK).[4] A crystallographic study demonstrated that a high-potential iron-sulfur protein (HiPIP) undergoes minor conformational changes upon toggling the redox state of the [4Fe4S] cluster between 2+ and 3+.[5] The coordinates of the atoms in the EndoIII protein structure for the $[4Fe4S]^{3+}$ case was therefore assumed to be the same as for the $[4Fe4S]^{2+}$ case. The authors in ref (5) suggested that the redox conversion at the [4Fe4S] metallocofactor induces electrostatic potential change at the

protein surface. The concept of redox-modulated binding affinity supports our proposed electrostatic model based on electrostatic interactions between DNA and [4Fe4S] DNA-processing proteins. The modeled ΔPE is ca. 7 kcal/mol, while the energy difference estimated from electrochemical studies is ca. 5 kcal/mol. Similar modeled ΔPE is also obtained for other DNA-processing proteins containing [4Fe4S] clusters or flavin cofactors, such as MutY, Dna2, and photolyase. The model ΔPE for MutY also recapitulates the energy difference between the 2+ and 3+ states computed from the redox potential shift obtained using electrochemical techniques.[6] This result corroborates that our electrostatic model is general and is readily applicable to other DNA-processing enzymes carrying [4Fe4S] metallocofactors.

Condition	# of Short DNA	# of Proteins on Short DNA	Proteins: Short DNA	# of Long DNA	# of Proteins on Long DNA	Proteins: Long DNA
< 1 % Ox - MM	280	496	1.77	49	174	3.55
< 1 % Ox - WM	139	185	1.33	31	49	1.58
33 % Ox - MM	140	192	1.37	23	55	2.39
33 % Ox - WM	372	428	1.15	69	100	1.45
66 % Ox - MM	352	594	1.69	49	134	2.73
66 % Ox - WM	375	473	1.26	76	129	1.70
> 99 % Ox - MM	169	210	1.24	25	39	1.56
> 99 % Ox - WM	108	137	1.27	22	30	1.36

Table S2. Number of DNA and proteins counted in the AFM redistribution assay using EndoIII oxidized to various extent.

Condition	r	dr
< 1 % Ox - MM	2.00	1.69
< 1 % Ox - WM	1.19	
33 % Ox - MM	1.74	1.38
33 % Ox - WM	1.26	
66 % Ox - MM	1.62	1.20
66 % Ox - WM	1.35	
> 99 % Ox - MM	1.26	1.17
> 99 % Ox - WM	1.07	

**Table S3**. Results of the AFM redistribution assay using EndoIII oxidized to various extent.

Table S2 shows the raw counting data. Table S3 utilizes the data in Table S2 and tabulates the calculated mismatched to well-matched differential as a function of the oxidation extent of EndoIII. The results show that as EndoIII becomes more oxidized, the ability to differentiate between WM and MM strands decreases (Figure 4).
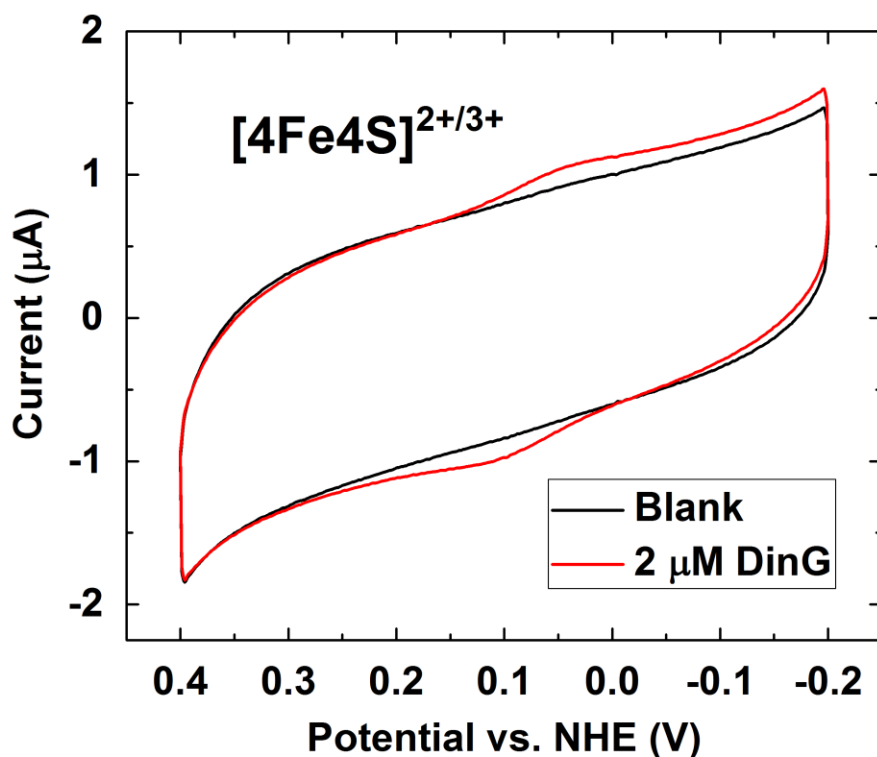
Figure S9. Cyclic voltammetry of DinG incubated with a DNA-modified electrode. CVs in protein buffer (20 mM NaH$_2$PO$_4$ pH 7.5, 100 mM NaCl, 5% glycerol, 1 mM EDTA, black line) with 2 μM DinG added (red line) at a scan rate of 100 mV/s.

Figures S9-10 displays CVs, SWVs, and DPVs of a DNA-modified Au electrode in protein buffer with and without DinG in solution. DinG exhibits a reversible redox wave with a midpoint potential of about +80 mV vs. NHE, a value similar to that observed previously by our group.[7,8] Only one redox peak is observed in the anodic and cathodic scans, indicating that only one electrochemical process is occurring.
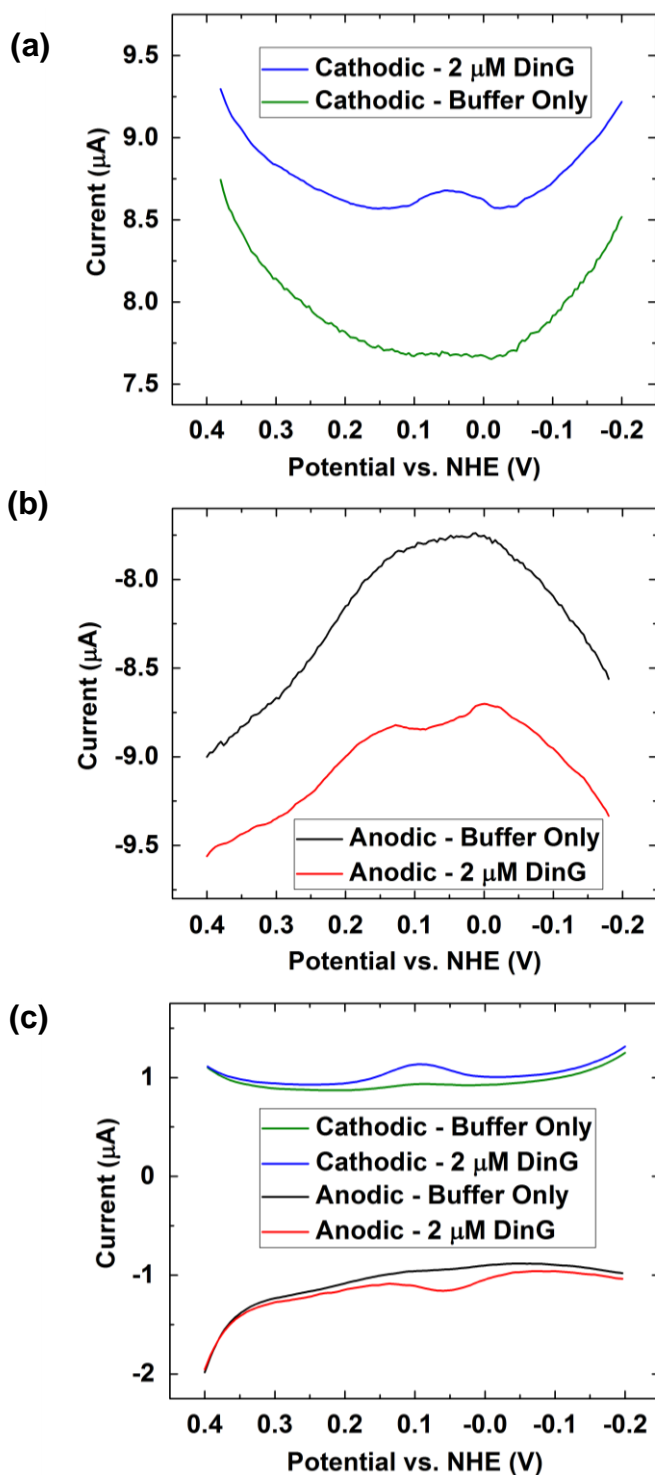
Figure S10. Square wave and differential pulse voltammetry of DinG incubated on a DNA-modified electrode. (a) Cathodic SWVs, (b) anodic SWVs, and (c) cathodic and anodic DPVs in protein buffer (20 mM NaH_2PO_4 pH 7.5, 100 mM NaCl, 5% glycerol, 1 mM EDTA) with 2 μM DinG added.
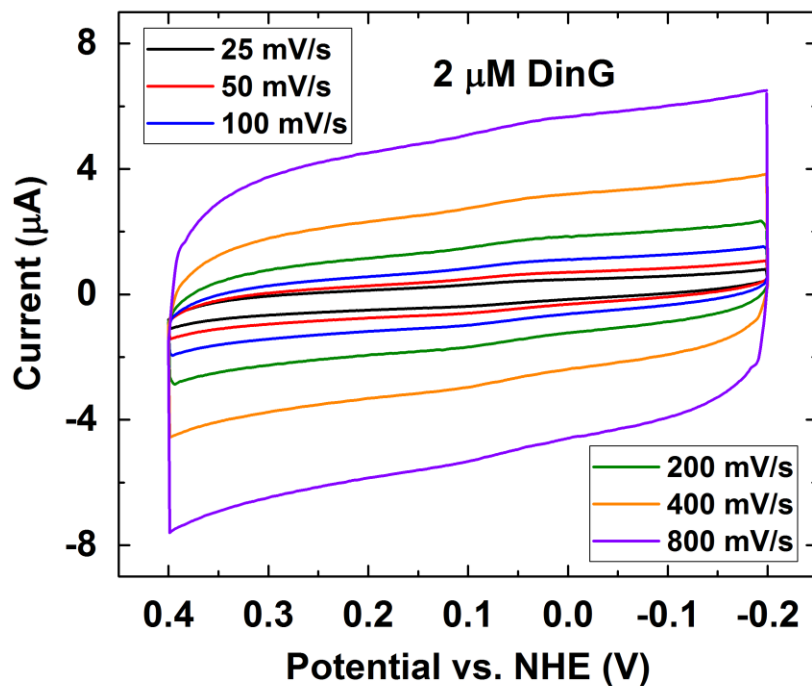
Figure S11. Cyclic voltammetry of DinG incubated with a DNA-modified electrode at different scan rates. CVs in 2 μM DinG in protein buffer (20 mM NaH_2PO_4 pH 7.5, 100 mM NaCl, 5% glycerol, 1 mM EDTA) at a scan rate of 25 (black), 50 (red), 100 (blue), 200 (green), 400 (orange), and 800 (purple) mV/s.

Figure S11 shows CVs of DinG at a constant concentration but at varying scan rate. Since the contribution of the capacitance to the total current is significant, the Faradaic component is extracted from the total peak current by removing the charging current prior to performing Randles-Sevcik analysis.
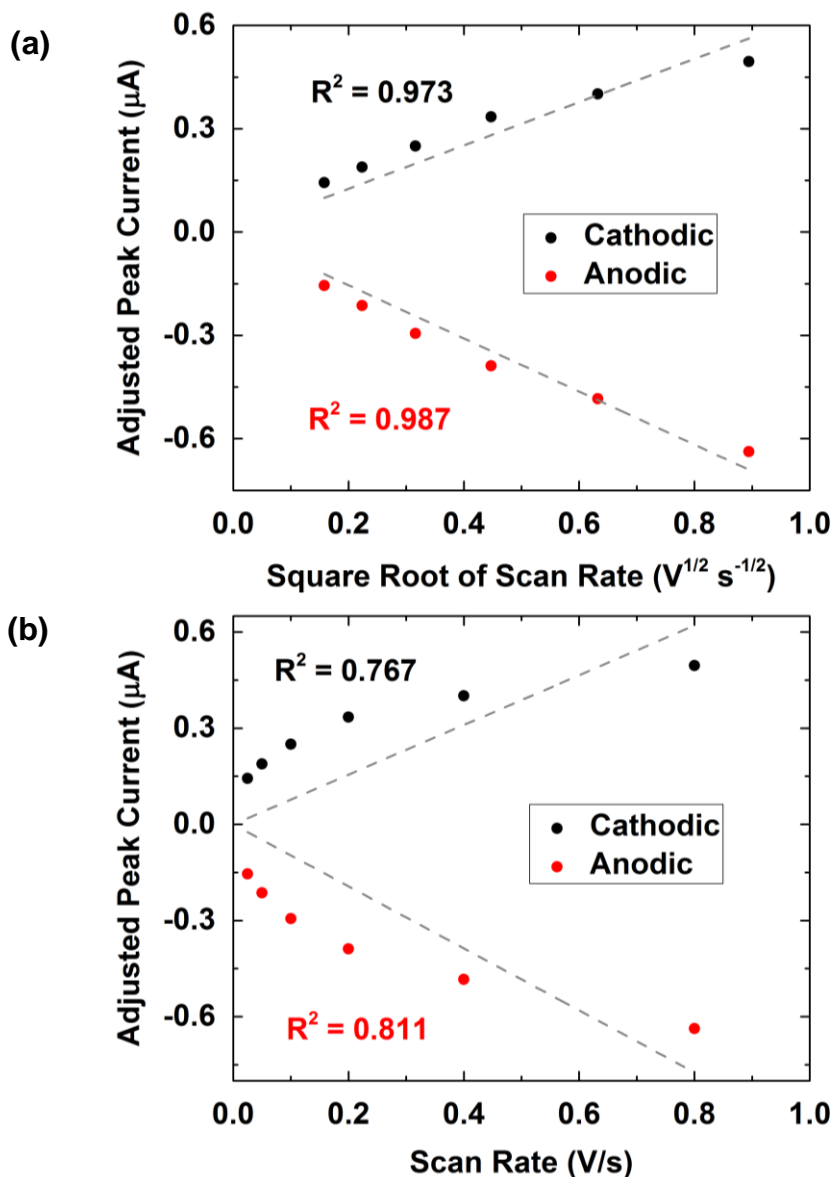
Figure S12. Randles-Sevcik plots of DinG electrochemistry. The background-subtracted peak currents of 2 μM DinG at various scan rates recorded in Figure S11 were plotted versus (a) the square root of the scan rate, and (b) the scan rate.

Figure S12a shows the Randles-Sevcik plot of DinG with the capacitance component of the peak current removed versus the square root of the scan rate. A linear correlation is observed for both the cathodic and anodic adjusted peak currents of DinG with the square root of the scan rate, indicating that the redox event involves a diffusive species. By contrast, Figure S12b shows a Randles-Sevcik plot of DinG with the charging-current-free peak current versus the scan rate. A

poor linear relationship is observed, corroborating that the redox event does not originate from an adsorbed species and that DinG does not associate very strongly to DNA under this condition.

Guided by the CV obtained in Figure S9 and the knowledge gained from the electrochemical characterization of EndoIII and DinG, we conducted bulk electrolysis on DinG at a constant oxidizing potential (+250mV vs. NHE) and reducing potential (−50mV vs. NHE) for 25 min. These potentials are chosen based on the positions of the anodic and cathodic peaks in Figure S9 in order to provide a thermodynamic driving force to generate cluster proteins in the $[4Fe4S]^{3+}$ and $[4Fe4S]^{2+}$ states, respectively.

(a)

(b)
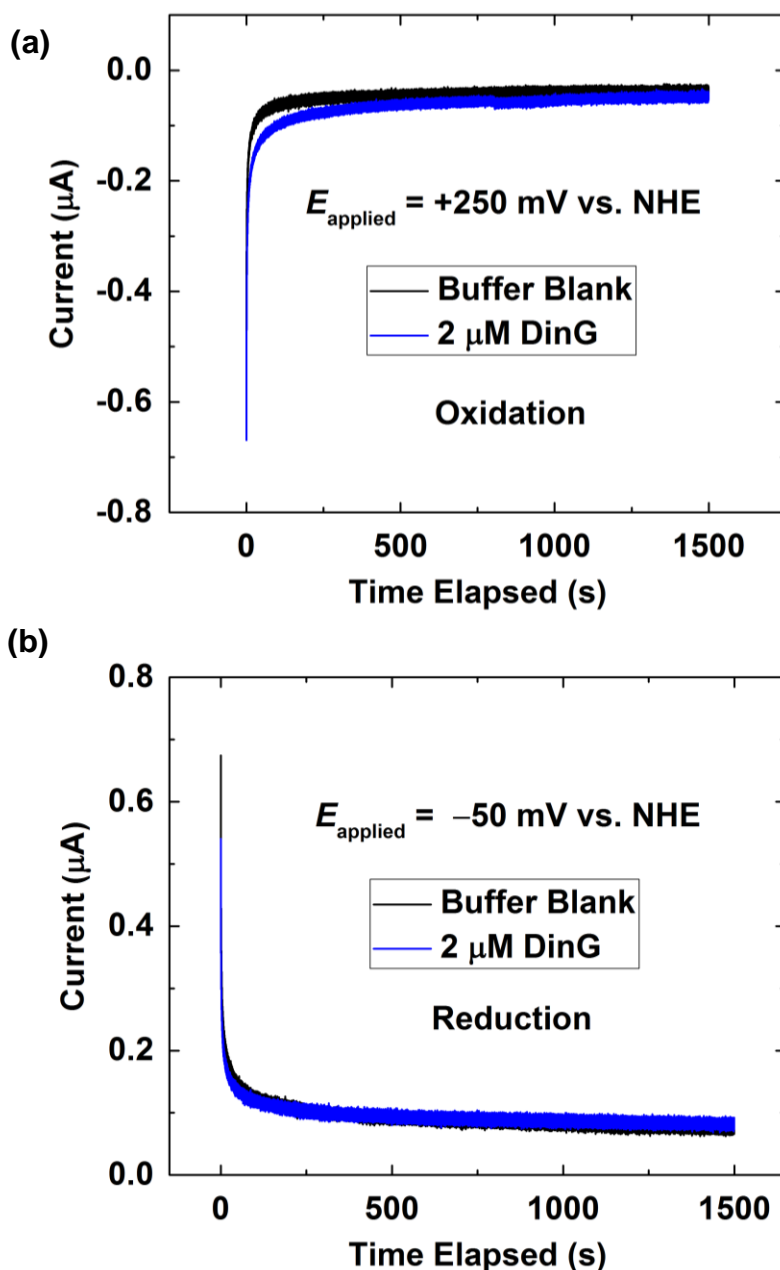
Figure S13. Bulk electrolysis of DinG using a DNA-modified electrode. Bulk electrolysis in protein buffer (20 mM NaH_2PO_4 pH 7.5, 100 mM NaCl, 5% glycerol, 1 mM EDTA, black lines) with 2 µM DinG added (blue lines) held at (a) +250 mV and (b) −50 mV vs. NHE.

Upon application of a positive potential in the presence of DinG, the magnitude of current recorded is larger than the buffer only case without DinG (Figure S13a, black and blue lines). Interestingly, the magnitude of current is very similar for both cases with and without DinG when

a negative potential bias is applied (Figure S13b, black and blue lines). These results suggest that native DinG likely contains a cluster that exists primarily in the reduced [4Fe4S]$^{2+}$ form. DinG is oxidized at +250 mV and reduced at −50 mV vs. NHE for all subsequent AFM studies.

Condition	# of Short DNA	# of Proteins on Short DNA	Proteins: Short DNA	# of Long DNA	# of Proteins on Long DNA	Proteins: Long DNA
< 1 % Ox - MM	1034	1003	0.97	50	86	1.72
< 1 % Ox - WM	781	765	0.98	47	50	1.06
> 99 % Ox - MM	719	637	0.89	48	81	1.69
> 99 % Ox - WM	742	1077	1.45	49	126	2.57

Table S4. Number of DNA and proteins counted in the AFM redistribution assay using reduced and oxidized DinG.

Condition	r	dr
< 1 % Ox - MM	1.77	1.63
< 1 % Ox - WM	1.09	1.63
> 99 % Ox - MM	1.90	1.08
> 99 % Ox - WM	1.77	1.08

Table S5. Results of the AFM redistribution assay using reduced and oxidized DinG.

Condition	# of Short DNA	# of Proteins on Short DNA	Proteins: Short DNA	# of Long DNA	# of Proteins on Long DNA	Proteins: Long DNA
33 % Ox - MM	817	801	0.98	53	100	1.89
33 % Ox - WM	791	790	1.00	54	73	1.35
66 % Ox - MM	542	471	0.87	63	104	1.65
66 % Ox - WM	775	865	1.12	49	80	1.63

Table S6. Number of DNA and proteins counted in the AFM redistribution assay using 33% and 66% oxidized samples which were prepared by mixing reduced DinG and oxidized EndoIII in a 2:1 and 1:2 ratios, respectively.

Condition	r	dr
33 % Ox - MM	1.92	1.42
33 % Ox - WM	1.35	
66 % Ox - MM	1.90	1.30
66 % Ox - WM	1.46	

Table S7. Results of the AFM redistribution assay using 33% and 66% oxidized samples which were prepared by mixing reduced DinG and oxidized EndoIII in a 2:1 and 1:2 ratios, respectively.

Condition	# of Short DNA	# of Proteins on Short DNA	Proteins: Short DNA	# of Long DNA	# of Proteins on Long DNA	Proteins: Long DNA
33 % Ox - MM	797	762	0.96	51	105	2.06
33 % Ox - WM	728	701	0.96	49	75	1.53
66 % Ox - MM	647	747	1.15	43	104	2.42
66 % Ox - WM	470	936	1.99	46	158	3.43

Table S8. Number of DNA and proteins counted in the AFM redistribution assay using 33 % and 66 % oxidized samples which were prepared by mixing reduced EndoIII and oxidized DinG in a 2:1 and 1:2 ratios, respectively.

Condition	r	dr
33 % Ox - MM	2.15	
33 % Ox - WM	1.59	1.35
66 % Ox - MM	2.09	
66 % Ox - WM	1.72	1.21

Table S9. Results of the AFM redistribution assay using 33 % and 66 % oxidized samples which were prepared by mixing reduced EndoIII and oxidized DinG in a 2:1 and 1:2 ratios, respectively.

Supplementary Experimental Procedures

(i) Isothermal Titration Calorimetry

Isothermal titration calorimetry (ITC) was carried out using a iTC200 MicroCalorimeter (MicroCal) at 21 °C. The DNA sequences used in ITC experiments were identical to the sequences used in MST experiments. For measurements of EndoIII primarily in the reduced state, native EndoIII (71 μM, 200 μL) was placed in the cell port and 21-mer (355 μM, 40 μL) was used as the titrant. For measurements of EndoIII primarily in the oxidized state, EndoIII (7.1 μM, 200 μL) was oxidized using a DNA-modified electrode in the glove bag previously described and the oxidized EndoIII solution was sealed in the glove bag with parafilm prior to transporting to the ITC instrument room. The oxidized EndoIII solution was then placed in the MicroCalorimeter cell port. 21-mer (71 μM, 40 μL) was used as the titrant. Residual glycerol in protein samples was removed via diafiltration using Ultracel centrifugal filters (10 kDa cutoff, Amicon Ultra). DNA titrant was dialyzed using Slide-A-Lyzer MINI dialysis units (2,000 MWCO, Thermo Scientific) against DNA buffer overnight, degassed with Ar, and centrifuged at 14,000 rpm to remove gas bubbles. Titrant was added in 16 successions (2.5 μL each) and the reaction mixture was allowed to equilibrate for 540 s between each addition. The stirring speed was kept at 1000 rpm.

DNA sequences used for ITC and EMSA measurements:

5'-ACT GAA CTC TGT ACC TGG CAC-3'

3'-TGA CTT GAG ACA TGG ACC GTG-5'　　　(complement)

(ii) Electrophoretic Mobility Shift Assay

Electrophoretic mobility shift assay (EMSA), also known as gel-shift assay, was conducted on radioactive hot benches. First, phosphorylation of the complement strand in the 21-mer (5 μM) used in MST and ITC experiments was carried out using radioactive [γ-32P]-labeled ATP (6000 Ci/mmol 150 mCi/ml Lead, 5 mCi, PerkinElmer) by T4 PNK (New England Biolabs) at 37 °C for 2 h and heat inactivated at 80 °C for 15 min. Radioactive 21-mer ssDNA was removed from the crude reaction containing unused ATP and denatured T4 PNK using Oligonucleotide Cleanup Kit (Monarch) by precipitating the 21-mer ssDNA onto the spin column using EtOH, then washed with 70% EtOH PE buffer solution for 3 times, and recovered using EB buffer (50 μL). Labeled 21-mer ssDNA was then gel-purified using a 20% polyacrylamide urea denaturing gel. The desired

21-mer ssDNA band was then visualized using an X-ray developer (Kodak) and excised using a razor blade. The excised band was re-dissolved in triethylammonium acetate buffer (TEAA, 100 mM, 1 mL) and incubated at 37 °C overnight. Water was removed from the reaction by SpeedVac and salt was removed by passing through Micro Bio-Spin 6 column (Bio-Rad) twice. Annealing titration between radio-labeled 21-mer complement strand and unlabeled 21-mer ssDNA that had been previously heated to 90 °C for 10 min and cooled to room temperature over a period of 3 h was conducted using 10% polyacrylamide native gel (Bio-Rad) at 4 °C and 50 V in 0.5X Tris/Borate/EDTA (TBE) buffer. Radioactively labeled 21-mer dsDNA was then degassed with Ar and incubated with native or oxidized EndoIII for 1 h in pH 7 DNA buffer with 20% glycerol to reach equilibrium under anaerobic condition. To quantify protein-DNA interaction, EMSA was then carried out using 10% polyacrylamide native gel (Bio-Rad) at 4 °C and 50 V in 0.5X TBE buffer inside the glove bag. The protein-DNA and DNA bands were transferred to a piece of Amersham Hybond-N nucleotide blotting paper (GE Healthcare) in transfer buffer (25 mM Tris-HCl, 200 mM glycine, 10% methanol, pH 8.5) using a HEP-1 Semidry Electroblotter (Thermo Scientific Owl). Exposure time was determined using a LS 6000SC Scintillation Counter (Beckman Coulter). The blotting film containing the transferred band was then exposed to a phosphorimaing storage screen (GE Healthcare) and imaged using a Typhoon FLA 9000 Imager (GE Healthcare).

(iii) DNA Sequences used in this Study

For EndoIII electrochemistry:

HS-C6-5'-GT GAG CTA ACG TGT CAG TAC-3'

      3'-CA CTC GAT TGC ACA GTC ATG-5'

For DinG electrochemistry:

HS-C6-5'- GT GCT GCA ACG TGT CTG CGC-3'

      3'-CA CGA CGT TGC ACA GAC GCG AGA GCA GAC GTC AGA-5'

For MST, ITC, and EMSA:

5'-ACT GAA CTC TGT ACC TGG CAC-3'

3'-TGA CTT GAG ACA TGG ACC GTG-5'

(HS-C6 = hexanethiol linker)

Supplementary References

(1) Pheeney, C. G.; Arnold, A. R.; Grodick, M. A.; Barton, J. K. *J. Am. Chem. Soc.* **2013**, *135*, 11869−11878.

(2) Cunningham, R. P.; Asahara, H.; Bank, J. F.; Scholes, C. P.; Salerno, J. C.; Surerus, K.; Munck, E.; McCracken, J.; Peisach, J.; Emptage, M. H. *Biochemistry* **1989**, *28*, 4450−4455.

(3) Webert, H.; Freibert, S.-A.; Gallo, A.; Heidenreich, T.; Linne, U.; Amlacher, S.; Hurt, E.; Mühlenhoff, U.; Banci, L.; Lill, R. *Nat. Commun.* **2014**, *5*, 5013.

(4) Thayer, M. M.; Ahern, H.; Xing, D.; Cunningham, R. P.; Tainer, J. A. *EMBO J.* **1995**, *14*, 4108−4120.

(5) Ohno, H.; Takeda, K.; Niwa, S.; Tsujinaka, T.; Hanazono, Y.; Hirano, Y.; Miki, K. *PLoS ONE* **2017**, *12*, e0178183.

(6) Bartels, P. L.; Zhou, A.; Arnold, A. R.; Nuñez, N. N.; Crespilho, F. N.; David, S. S.; Barton, J. K. *Langmuir* **2017**, *33*, 2523−2530.

(7) Grodick, M. A.; Segal, H. M.; Zwang, T. J.; Barton, J. K. *J. Am. Chem. Soc.* **2014**, *136*, 6470−6478.

(8) Romano, C. A.; Sontz, P. A.; Barton, J. K. *Biochemistry* **2011**, *50*, 6133−6145.